JOURNAL OF SOFT COMPUTING AND DATA MINING
e-ISSN: 2716-621X

JSCDM

Vol. 6 No. 1 (2025) 359-377
https://publisher.uthm.edu.my/ojs/index.php/jscdm

LSOARP: A Link Stability and Obstacle-Aware Routing Protocol for UAV Networks

Almuntadher Mahmood Alwhelat[1,2]*, Muhammad Ilyas[3,4], John Bush Idoko[2], Lina Jamal Ibrahim[2], Mazin S AL-Hakeem[1], Sinan Q. Salih[5]

[1] *Department of Computer Engineering, Al-Farabi University College, Baghdad, 10022, IRAQ*
[2] *Applied Artificial Intelligence Research Centre, Department of Computer Engineering, Near East University, Mersin-10, 99138, TURKEY*
[3] *College of Engineering, Department of Cybersecurity, Al Ain University, Abu Dhabi, 61414, UAE*
[4] *Department of Computer Engineering, Altinbas University, Istanbul, 34217, TURKEY*
[5] *Technical College of Engineering, Al-Bayan University, Baghdad 10011, IRAQ*

*Corresponding Author: almuntadher.mahmood@alfarabiuc.edu.iq
DOI: https://doi.org/10.30880/jscdm.2025.06.01.024

Article Info

Received: 13 May 2025
Accepted: 8 June 2025
Available online: 30 June 2025

Keywords

FANET, UAV, Bezier curves, obstacles, energy, routing, energy efficiency

Abstract

As using Unmanned Aerial Vehicles (UAVs) continues to grow across military, environmental, and public safety sectors, we are seeing a fast development of Flying Ad Hoc Networks (FANETs). Despite this progress, creating reliable routing protocols for UAVs remains complex because of their high mobility, constantly changing network topology, frequent link drops, and physical obstacles in the environment. Current protocols often overlook the importance of link stability and obstacle-aware navigation, which can lead to decreased performance in real-world applications. we present LSOARP: a Link Stability and Obstacle-Aware Routing Protocol customized for UAV networks. This new protocol combines Bézier-curve-based trajectory adjustments for better obstacle avoidance with a multi-criteria link evaluation that considers residual link lifetime, energy efficiency, and route availability. We model UAV movement using a realistic prediction mechanism that captures various states such as high, low, idle, and paused. Routing decisions are then made using a weighted cost function to select the most stable and energy-efficient paths, ensuring strong network performance. Simulation experiments conducted under different conditions—including varying node density, speed, pause times, and traffic loads—show that LSOARP considerably outperforms traditional protocols like RLPR and AODV. It offers higher packet delivery ratios, lower end-to-end delays, reduced energy consumption, and less control overhead. These promising results demonstrate that LSOARP is both scalable and reliable in complex UAV environments, making it a strong candidate for real-time FANET applications.

1. Introduction

A Flying Ad-Hoc Network (FANET) is a network comprising a swarm of Unmanned Aerial Vehicles (UAVs) facilitating wireless communication. The nodes efficiently retrieve data from databases. [1]. UAVs and anointed drones are also gaining prominence in essential applications such as military operations. Commercial and applications relating to academic research. [2]. The advancement of technology and widespread accessibility of reduced-cost appliances have opened the way for the development of FANETs.

FANET groups trivial drones in an ad hoc way [2]. A network of drones can be coordinated and synchronized to execute a task assigned by the Ground Control Station (GCS) [3]. FANETs organize themselves and offer reduced-cost, flexible, and simple-to-instrument flying nodes, permitting them to finish complex duties faster and cooperatively. One of the key challenges in FANETs is the increased power consumption at the node. Advanced node. Nodes in the FANET should consume reduced power. The cost of FANET and its performance rely on the energy each flying node uses. [4][5]. Advanced mobility with particularly active topology poses obstacles to communication methods, mainly throughout the design process of a routing protocol for UAV-based wireless networks [4].The FANET includes exclusive features like movement in a 3D space, increased mobility, recurrent topological variations, inadequate resources, reduced node densities, and so on, which enforce numerous Difficulties in constructing an effective routing mechanism [5].

A significant challenge in managing the mobility of drones is the presence of obstacles, consisting of trees, structures, etc., that obstruct radio transmission signals and influence the FANET's function or efficiency based on throughput, latency, and connectivity. As UAVs are proactive, they can change their route easily, as in the case of FANETs. This requires effective routing to specify a fluffy network connection [6]. UAVs must communicate among themselves and with the (BS) through an adequate routing protocol [7]. Organizing an effectual multi-hop routing protocol is challenging for increased mobility, live topology, limited power, and reduced communication coverage. MUlti-objective optimization mechanisms like evolutionary schemes propose better consequences. Designing an efficient routing protocol is a challenge for FANETs owing to the dynamic nature of UAVs [5].

The rest of the paper is organized as follows: Section II reviews some recent works related to routing in FANETs. Section III details the proposed Protocol. In Section IV, we present and discuss the experimental results. Finally, the paper wraps up with the conclusions in Section V. This study introduces a new protocol called the Obstacle Aware and Link Stability-based Position Routing, or LSOARP.

The proposed scheme outperforms state-of-the-art schemes like RLPR [21] and AODV [22] in the duration of wavering energy, Packet Delivery Ratio (PDR), speed, etc.

2. Related Work

This section examines various routing strategies specifically tailored for Flying Ad Hoc Networks (FANETs) and analyses how different authors have addressed the unique challenges of creating efficient and reliable communication paths in these dynamic aerial networks.

2.1 Routing Schema in FANET

Changing the network topology quickly can impact how well routing protocols work in FANETs. Hong & Zhang (2019) [8] have proposed a routing mechanism appropriate for extremely dynamic MANETs that supports rapid topology changes in complex scenarios. In the offered mechanism, mobile nodes observe deviations of adjacent topology sporadically, and the current method is confirmed based on the apparent outcome. Moreover, an appropriate routing protocol is chosen to preserve the network performance at an elevated level. The evaluation focuses on packet delivery ratio (PDR), productivity, average latency, and jitter. The random waypoint, starting point collection mobility, and pursuit models are interconnected, managing significant fluctuations in network structure. The results indicate that a suitable routing mechanism can adjust to quick variations in network topology and efficiently improve network execution. The scheme fails to consider the weight elements among the causing ones. The topology change threshold must be determined.

Lee et al. (2021) [9] introduced a two-step routing system that uses Fuzzy Logic (FL) to help make smarter decisions about how data moves through the network. specifically, route detection and route servicing. Initially, a scheme is proposed for computing the node scores to overcome the issue of a broadcast storm and overflowing of Control messages disseminated to ascertain a path. This score is computed. depending on numerous parameters like the direction of motion, this includes the residual energy (RE) of nodes, the quality of links, and how stable each node is. the selection of routes, a fuzzy system is designed to choose routes with increased fitness, reduced delay, and fewer bounds for transferring data. Secondly, route collapses must be overcome by identifying and altering paths at the collapse threshold and rebuilding botched routes to know and rapidly supersede these paths. The outcomes of the schemes are compared with those of ECaD, LEPR as well as AODV. The results clearly indicate that the scheme outdoes other routing mechanisms based on end-to-end latency, PDR, route stability, and the amount of energy devoured. Nevertheless, the routing overhead has improved. Similarly, Kumar et al. (2022) [10]

introduced a routing approach that takes into account both mobility and link stability, using adaptive thresholds to ensure reliable communication even in highly energetic UAV environments. Their research emphasizes the significance of incorporating mobility prediction into routing decisions to enhance overall network robustness.

2.2 Position-centric Routing Strategies in FANET

In contrast to topology-dependent routing, position-dependent routing exists. Illustrates increased effectiveness and agility in distributing with the increased mobility of nodes. Oubbati et al. (2017) [11] have completed an Analysis of position-dependent routing methods across several categories. A classification and taxonomy of protocols and a comprehensive discussion of routing methods within each category are provided. A relative study is carried out depending on numerous criteria, along with the merits and disadvantages of every protocol. There is coordination among drones (UAVs) and Vehicle-to-Vehicle networks (VANETs) are technologies that operate on the ground. They play important roles in modern transportation and communication systems. Tolerance is also a key concept in ensuring these systems work smoothly and safely.
should be taken into consideration.

To deal with service scenarios, a communication path must be preserved among GCS and UAVs, and UAVs must be capable of exchanging messages. Nevertheless, their communication reach is restricted based on transceiver power and delicate. A multi-hop network scheme should be considered, with a dominant routing protocol. Choi et al. (2018) [12] have proposed a geolocation-dependent routing protocol that offers robust, and the system maintains strong performance even as the network topology changes quickly, thanks to the faster movement of UAVs during task execution. The protocol utilizes the neighbors' geolocation information and then determines the route to a destination by taking the neighbors' information, resulting in reduced overhead and stability in the dynamic topology. What's more, Zhang et al. (2023) proposed a position-based protocol that blends geolocation with obstacle avoidance, aiming to improve route dependability in urban UAV operations.[13]
Position-dependent routing algorithms are deemed appropriate for routing in FANETs due of the UAV's geographical data is available.

Kumar et al. (2021) [14] have dealt with the adaptation of Location-Aided Routing (LAR) called 3D Cone-shaped LAR (3DC-LAR). Route discovery this process is done through a request zone in the current LAR system.wherein nodes in the appeal zone forward route requests for transferring data. The proposed mechanism changes the description of the request zone using a three-dimensional form by Midway UAVs. The results indicate that the mechanism exhibits diminished routing above.

2.3 Obstacle-Aware Routing Schemes in FANET

To handle obstacles, Gankhuyag et al (2017) [15] have proposed a joint Omni-directional as well as directional transmission mechanism along with dynamic angle alteration. The proposed mechanism supports the hybrid employment of unicast and geo-cast routing based on position and route data. The mediator node positions are predicted using a 3-D assessment and indicator broadcast to the forecast position, supporting a lengthier transmission range and keeping track of fluctuating topology that guarantees the protocol's robustness. Additionally, drop-in route restoration and Duration of service disruption for enhancement path lifetime and effective packet communication guarantee the trustworthiness of the recommended approach.
Kim et al. (2017) [16] focused on quickly recovering multi-drone ad hoc network surroundings. The proposed mechanism with a non-recovery setting confirms that the proposed mechanism outperforms based on PDR and requires a disconnection schedule.

Sorbelli et al. (2022) [17] proposed a multi-drone management and networking system that relies on obstacles and energy and employs a location-based reinforcement learning (RL) system prediction mechanism along with a packet forwarding scheme for the drone-to-ground formation of the network. Drone location-based heuristic greedy and learning-dependent explanations are offered and designed for forwarding envelopes to deliver diverse Performs depending on implementation requirements. The requirements demand improving connectivity by on adjusting PDR and reducing end-to-end delays, especially when there are obstacles around, to make things work more smoothly and efficiently. Efficiency by dropping the amount of energy and time consumed, irrespective of energy constraints. The suggested mechanism is executed on a track-dependent testbed for DRM FANET. The expected method circumvents barriers and proposes 81-90% communication without obstacles.
Schemes focusing on several factors, which include communication, mobility, energy, constancy etc., are needed for efficient routing in VANET.

3. Link Stability and Obstacle-Aware Routing Protocol for UAV Networks (LSOARP)

Protocol of (LSOARP) is proposed for routing in FANET in the presence of obstacles. “DeCasteljau’s algorithm” based upon the Bézier curve is a smooth, curved line used in designing paths and computer graphics. It's created using a set of control points, which gives you a lot of flexibility in shaping the curve. This makes it really handy for

generating paths around obstacles or in tricky navigation situations.[18] is used in support of mobility. Energy-aware optimal routing behaved in predicting mobility, energy, link reliability, connectivity as well as path availability. Recent studies, such as the work by Raj and Gupta (2021), have integrated obstacle prediction into UAV path planning. They use terrain analysis combined with sensor feedback to dynamically optimize flight trajectories, even under real-time constraints. [19]

3.1 Obstacle Aware Routing

That aims to qualify node motion with collision-free and obstacle restraints in practical application scenarios is developed the "DeCasteljau Algorithm" (RMDA) is the foundation of the realistic mobility model.
RMDA algorithm steps, which are the method addressed in Algorithm 1, pertain to identifying node mobility amongst disparate impediments and collision-free limitations in a real-time environment.
RMDA can encounter various practical scenarios by considering mobility among straight lines, general curves, and circle lines.

There may be dissimilar geographical restraints induced by obstacles, including vegetation, cars, and buildings, that block a Mobile Node's (MN's) path in the area. Moreover, an MN may encounter unequal obstacles through unsystematic shapes in real-time situations. It implies that MNs should move alongside the obstacles in an even route, utilizing a common curve instead of a straight route.

The MN (N_j) initially placed at 'PN_i^j' in the 'i^th' step is allotted a random destination 'PN_(i+1)^j'. It then moves towards 'PN_(i+1)^j' at a tangent speed. 'v_i^j' that is uniformly distributed between '[v_min,v_max]'. Assume that an irregular obstacle exists among 'PN_i^j' and 'PN_(i+1)^j'. The obstacles center point is denoted by 'OC_i' and radius is.

To evade collocating along the route from 'PN_i^j' to 'PN_{i+1}^j', 'N_j', a Bezier curve is used shown in Figure 1 that permits through a control point signified as 'PN_i^{j*}'. The waypoints 'PN_i^j' and 'PN_{i+1}^j' in the 'i^{th}' step is represented as two 2D coordinates (X_i^j, Y_i^j) and (X_{i+1}^j, Y_{i+1}^j) correspondingly. Figure 1 shows how Bézier curves help UAVs avoid obstacles. The path around an obstacle is smoothly shaped using control points, making the detour natural and easy to follow. This approach is a key part of LSOARP's way of navigating, helping UAVs move safely through areas filled with physical barriers.

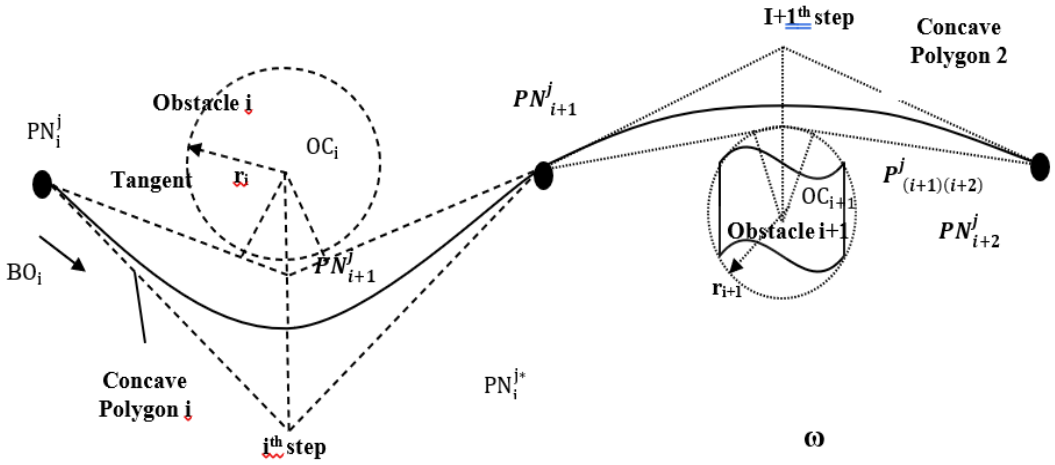

Fig. 1 *Obstacles with Bezier curves*

The step curve followed by 'N_j' moving from 'PN_i^j' to 'PN_{i+1}^j' includes a collection of points as shown in Eq. (1)

$$\begin{bmatrix} X_j \\ Y_j \end{bmatrix} = \Sigma_{k=0}^{3} \begin{bmatrix} X_k^j \\ Y_k^j \end{bmatrix} B^3 k \tau^k (i-\tau)^{3-k} \quad (1)$$

where,
$\tau \in [0,1]$ - Curve factor whose value is 0 and 1 initially
PN_i^j and PN_{i+1}^j - Goal waypoints in the 'i^{th}' step
B^3k - Bernstein polynomials of degree 3

'PN_i^{j*}' the adjust point emphasized here is so important because it helps determine how the step curve section forms.

When non-distinct obstacle constraints are present along the path, 'PN_i^{j*}' is jointly determined by using 'OC_i' and 'r_i'. With knowledge about obstacles and the allocated destination, the node 'N_j' can move on the step curve section. 'PN_i^{j*}' can be computed by solution for figuring out the meeting point represented by '$P_{i,i+1}^j$'. The two lines '$\overline{PN_i^j P_{i,1}^j}$' and '$\overline{PN_{i+1}^j P_{i,2}^j}$'intersect within 'ω'. The lines are tangential to the spherical obstacle boundary at points denoted by '$P_{i,1}^j$' and '$P_{i,2}^j$' respectively that are jointly decided by 'OC_i, r_i'.and the related waypoints. The border of 'i' represented by 'BO_i' can be around characterized as $(x - x_i)^2 + (y - y_i)^2 = r_i^2$, where (x_i, y_i) is the 2D formatting of 'OC_i'.

The collision-free choice to build fresh via points is determined if $CS_i^j \cap BO_i = \emptyset$. However, there are many possible points to make 'CS_i^j' on the stretched line of '$\overline{OC_i P_{i+1}^j}$'.
The output segment reduces the cost function 'c_j'. Strictly,

$$c_j = \sigma \int_{X_i}^{X_{i+1}} \int_{Y_i}^{Y_{i+1}} |k(x,y)|\, dx.\, dy + (1-\sigma) \int_{X_i}^{X_{i+1}} \int_{Y_i}^{Y_{i+1}} |\, CS^j\ x.y \tag{2}$$

were,
$\sigma \in [0,1]$ - Constant
k(x, y) - Curve of the part
I_i^j - Centre among obstacles

The reduction of 'c_j', 'CS^j' has a trade-off between smoothness degree and safety by an option of 'σ.' Once MN reaches 'PN_{i+1}^j' and finishes a round trip on 'CS^j' in 'i^{th}' step, it arbitrarily selects the ensuing destination. 'PN_{i+2}^j' for '$i + 1^{th}$' step, also thus forth. The control point series is broken into numerous subsequences to create piecewise Bezier curves in every step, and the piecewise curves are linked to establish the complete curve.
The whole movement trace of MN, 'N_j' is an arrangement of Several paths that can be shown by $\{CS_1^j, CS_2^j, \ldots\ldots CS_i^j\}$..

Algorithm 1: RMDA (Obstacle Detection)

Input:
$N_1, N_2, \ldots N_n$ - Number of nodes (n)
$O_1, O_2, \ldots O_s$ - Number of obstacles (s)
ω - 2D- Rectangular movement range
$PN_1, PN_2, \ldots PN_m$ - Number of waypoints (m)
Output: $\cup_{j=1}^{N} \cup_{i=1}^{M} CS_i^j$ - Movement trajectories of MN

Steps:
For N_j $//I \geq j \leq N$
For PN_i $//I \geq i \leq M$
If 'N_j' pauses, it stays at 'PN_i' accompanied by coordinates 'X_i^j, Y_i^j' for pre-determined pause time

Else
'N_j' chooses a next point 'PN_{i+1}' with 'X_i^{j+1}, Y_i^{j+1}' within 'ω'
'N_j' moves to 'PN_{i+1}' according to speed 'v_i^j', where $v_i^j \in [v_{min}, v_{max}]$
If there are unexpected obstacles in the way, and the object needs to maneuver around them,'PN_i' and 'PN_{i+1}', 'N_j' move around the obstacles

For 'O_k' $//1 \leq k \leq S$
Calculate the control position. 'PN_i^*' which is determined by 'O_k' has a radius 'r_k'
Derive Bezier curve segment.
$CS_i^j = \{X, Y | (x,y) = \in PN_i^j + (1-\in) PN_{i+1}^j\}_{i+1}$

$$\begin{bmatrix} X_j \\ Y_j \end{bmatrix} = \sum_{k=0}^{3} \begin{bmatrix} X_k^j \\ Y_k^j \end{bmatrix} B^3 k^{\tau k} (i-\tau)^{(3-k)}$$

Minimize the cost function. 'f_c' so that it is as smooth as possible

$$c_j = \sigma \int_{X_i}^{X_{i+1}} \int_{Y_i}^{Y_{i+1}} |k(x,y)|\, dx.\, dy + (1-\sigma) \int_{X_i}^{X_{i+1}} \int_{Y_i}^{Y_{i+1}} \left|CS_i^j - I_i^j\right| dx.\, dy$$

Else

$CS_i^j \cap BO_i = \emptyset$ and $CS_i^j = \overline{PN_i^J P_{i+1,J}^J}$ //'N_j' moves to 'PN_{i+1}' along the straight line

A sample representing this movement is shown in Figure 2 provides a clear overview of how the RMDA algorithm intelligently handles obstacle avoidance. It shows how the UAV assesses the environment for obstacles and, when necessary, plans a smooth detour using Bézier curves before resuming its course toward the waypoint. In Figure 3, the mobile node 'n_i' moves in every step curve section from a starting point to a destination in the field (ω)

As well as eight unequal obstacles (01 – 08). In this paper, the nodes using Random Way Point (RWP) exhibit and the obstacles are presented in the 'ω' realistic situation, and the simulation time taken is 60 seconds. Assuming there is no obstacle to stopping the motion of a mobile node in this instance, the trajectory towards the destination should transition from a generic curve to a specialized curve to minimize trip time. as well as the quantity of energy spent in FANET. Figure 3 illustrates how the UAV node moves through a variety of obstacles within the simulated environment, displaying how LSOARP intelligently adjusts its paths on the fly by employing piecewise Bézier curves in environments with many obstacles.

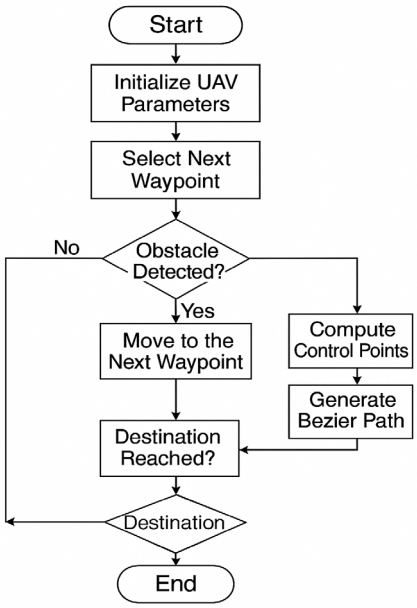

Fig. 2 *RMDA (obstacle detection)*

This flowchart shows in Figure 2, how UAVs navigate while being aware of obstacles, based on what's outlined in Algorithm1 (RMDA). The UAV begins by setting up its movement settings and choosing the next point to go to. Then, it checks if there are any obstacles in its direct path. If the way is clear, it heads straight to the next point. If obstacles are detected, the UAV calculates control points and creates a Bezier curve to go around them. It follows this curve, then checks if it has reached its destination. This process repeats until the UAV finally arrives at its last waypoint.

3.2 Efficient Routing Considering Mobility, Energy Use, Link Reliability, Connectivity, and Path Availability

This section covers path accessibility aware optimal routing, mobility, energy, connectivity, and link trustworthiness.

J. of Soft Computing and Data Mining Vol. 6 No. 1 (2025) p. 359-377

3.2.1 Mobility Prediction

(LSOARP) employes a random mobility model for nodes moving, and the prediction of Mobility is conducted to assess the accessibility of nodes inside the network. The Probabilistic Density Function (PDF) is utilized to ascertain the relative velocity of the node. Node movement results in many states such as:

H_φ - High speed
I_ω - Idle speed
L_ρ - Low speed
P_δ - Pause state

Movement of nodes is denoted as $X = \{H_\varphi, I_\omega, L_\rho, P_\delta\}$. In these states, the nodes moving speed (N_S) consistently accelerate from 0 to 'N_S'. Node actions are represented using diverse notations like $\{T_0, D_y, a_y, \lambda_y\}$.

were,
T_0 - Initial time of node motion

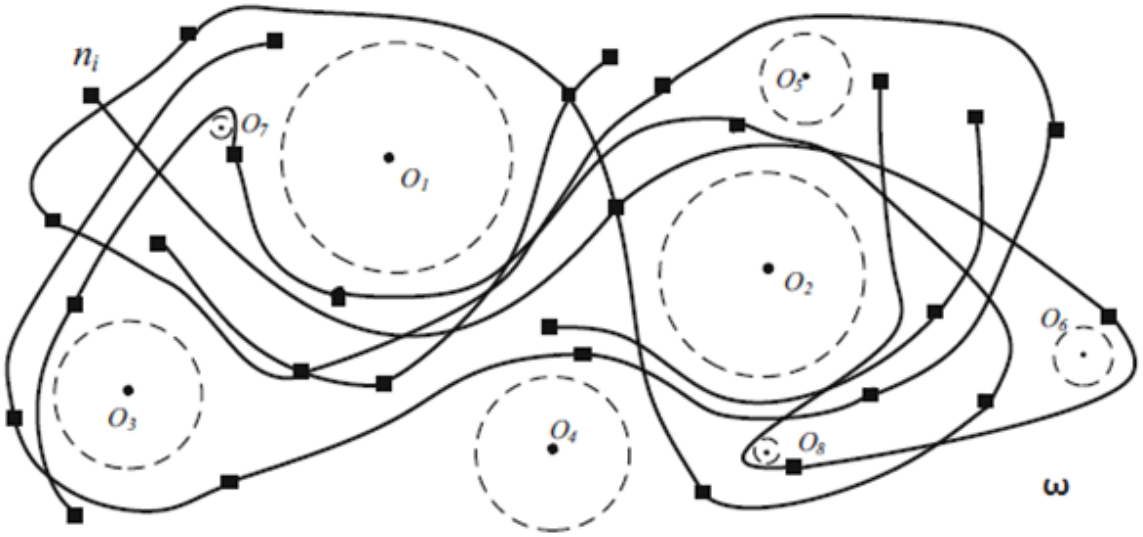

Fig. 3 *The mobility of mobile nodes across obstacles in FANETs*

λ_y - Duration of node mobility
D_y - Node movement directions
a_y - Node acceleration
High-Mobility State ($\boldsymbol{H_\varphi}$)
If '$T_\varphi = T_0 + \lambda_\varphi$', the time boundary of node value is given by $\{T_0, T_\varphi\}$.

In 'H_φ', primarily if the If the node's velocity is '0', it is then continually accelerated. N_(s_min) When the probability of velocity boundary position among. '$N_{s_{min}}$' and '$\{N_{s_{min}} + \Delta N_s\}$' is signified by '$\{N_{s_{min}} + \Delta N_s\}$'. The expression $\left\{\frac{1-\Delta N_s}{N_{s_{max}} - N_{s_{min}}}\right\}$ indicates the value of '$\{N_{s_{min}} + \Delta N_s\}$'.
The PDF of speed is expresses as given below.

$$r_v^{\varphi}(N_s) = \begin{cases} \frac{2}{N_{s_{min}} + N_{s_{max}}}, 0 \le N_s \le N_{s_{min}} \\ \left(\frac{2}{N_{s_{min}} + N_{s_{max}}}\right) * \left(\frac{N_{s_{max}} - N_s}{N_{s_{max}} - N_{s_{min}}}\right), N_{s_{min}} \le N_s \le N_{s_{max}} \end{cases} \quad (3)$$

Idle speed ($\boldsymbol{I_\beta}$)

The nodes proceed beside a straight line ($D_{\omega E}$) at a node speed of '$N_{s\omega}$' and the genuine trajectory is permitted to marginally diverge from '$D_{\omega E}$' at a certain point in the movement, it's important to recognize when nodes

smoothly transition from one state to another.'H_φ' to 'I_ω' of direction among '$D_{\omega E}$' and 'D_φ' should be in 'D_d^ω' and must be more than 0. The memory degree is represented by 'Ω' and the margin is ($\Omega \in (0,1)$) that lies concerning '$N_{s\omega}$' and '$N_{s\varphi}$'.

Were,

$$\lambda_\omega \sim U(\lambda_{\omega_{min}}, \lambda_{\omega_{max}}) \quad (4)$$

$$D_{\omega E} \sim U(N_{s_\varphi} + D_d^\omega, D_\varphi - D_d^\omega) \quad (5)$$

Were,
V0 - Gaussian variable belonging to N (0,1)
The preliminary speed of the node '$I_\omega(N_{s_0}^\omega)$' equal 'N_{s_φ}' and 'N_{s_ω}'.

$$I_\omega = \Omega N_{s_0}^\omega + (1-\Omega) * N_{s_\varphi} + \sqrt{1-\Omega^2 V_0} \quad (6)$$

$$I_\omega = N_{s_\varphi} + \sqrt{1-\Omega^2 V_0} \quad (7)$$

The idle speed is computed depending on the former analysis as in Equation (4).

$$r_v^\omega(N_s) = \frac{G\left(\frac{N_s - N_{s_{min}}}{\sqrt{1-\Omega^2}}\right) - \left(\frac{N_s - N_{s_{max}}}{\sqrt{1-\Omega^2}}\right)}{N_{s_{max}} - N_{s_{min}}} \quad (8)$$

$$G(x) = \frac{1}{\sqrt{2\pi}} \int_{-\alpha}^{x} \exp\left(\frac{-y^2}{2}\right) dy \quad (9)$$

The main variance among 'I_ω' and Middle Smooth (MS) stage is that 'I_ω' exclusively uses (4) to modify '$r_v^\omega(N_s)$' for entire stage duration, while MS model includes 'I_ωThe Gauss-Markov process is a multiple-phase process.

Low Speed ($\boldsymbol{L_\rho}$)
In 'L_ρ', the speed of node motion (N_s) is reduced consistently as '$N_{s_0}^\rho$' to 0. Node transition takes place from 'T_ω' to 'T_ρ'. The time interval is given by $T_\rho = T_\omega + \lambda_\rho$ and the duration ranges between $\lambda_\rho \sim U(\lambda_{\rho_{min}}, \lambda_{\rho_{max}})$.
$N_{s_0}^\rho$ - Movement from initial state (L_σ) and final state (I_β)
$D_\rho \sim U(D_{\omega E} + D_d^\rho, D_{\omega E} - D_d^\rho)$

Where,
D_d^ρ - Diverges from 'D_ρ' and '$D_{\omega E}$'.
Let,

$$V_0 = \sqrt{1-\Omega^2 V_0}, \text{ then } V_0^\sigma \sim N(0, 1-\Omega^2) \quad (10)$$

Where,
'V_0^σ' is determined by 'N_{s_φ} (1)'.
It is assumed reasonably that. 'V_0^ρ' is also regularly distributed as. 'N_{s_φ}'.
Based on '3-ρ' principle, if $h \sim N(\mu, \rho^2)$, the chance of 'h' falling outside (μ-3ρ, μ+3ρ) is fewer than 3%.
Since 'L_σ' has symmetric possessions with 'Hα', '$r_v^\varphi(N_s)$' can be derived as shown in the following equation.

$$r_v^\varphi(N_s) = \begin{cases} \frac{2}{N_{s_{min}} + N_{s_{max}}}, 0 \le N_s \le N_{s_{min}}^{Low} \\ \left(\frac{2}{N_{s_{min}} + N_{s_{max}}}\right) * P\left(V_0^\rho \ge N_S\right), N_{s_{min}} \le N_s \le N_{s_{min}}^{High} \end{cases} \quad (11)$$

Where,

$$N_{s_{min}}^{Low} = N_{s_{min}} - 3 * \sqrt{1-\Omega^2} \quad (12)$$

$$N_{s_{min}}^{High} = N_{s_{max}} + 3 * \sqrt{1-\Omega^2} \quad (13)$$

'V_0^ρ' is only 'L_ρ' state and will haven't an impact '$r_v^\omega(N_s)$' for 'I_ω'.
Pause State ($\boldsymbol{P_\delta}$)

In this pause, state (P_δ), the nodes pause for an arbitrary interval [t_ρ,t_δ] where $t_\rho \sim U(t_{\rho_{min}}, t_{\rho_{max}})$, $t_\delta = t_\omega + t_\rho$ before resuming a fresh moving cycle.

The movement of drones, or UAVs, is described through four main states: high-speed (Hφ), idle (Iω), low-speed (Lρ), and pause (Pδ). In the states where the UAV is moving—high, idle, or low speed—its acceleration is

J. of Soft Computing and Data Mining Vol. 6 No. 1 (2025) p. 359-377

calculated by dividing its velocity by the time spent in that state. Both the speed and the time are randomly chosen from uniform distributions, which helps to mimic the natural variations in how drones move. This approach enables the model to produce smooth shifts and more realistic flying behaviors between different states.

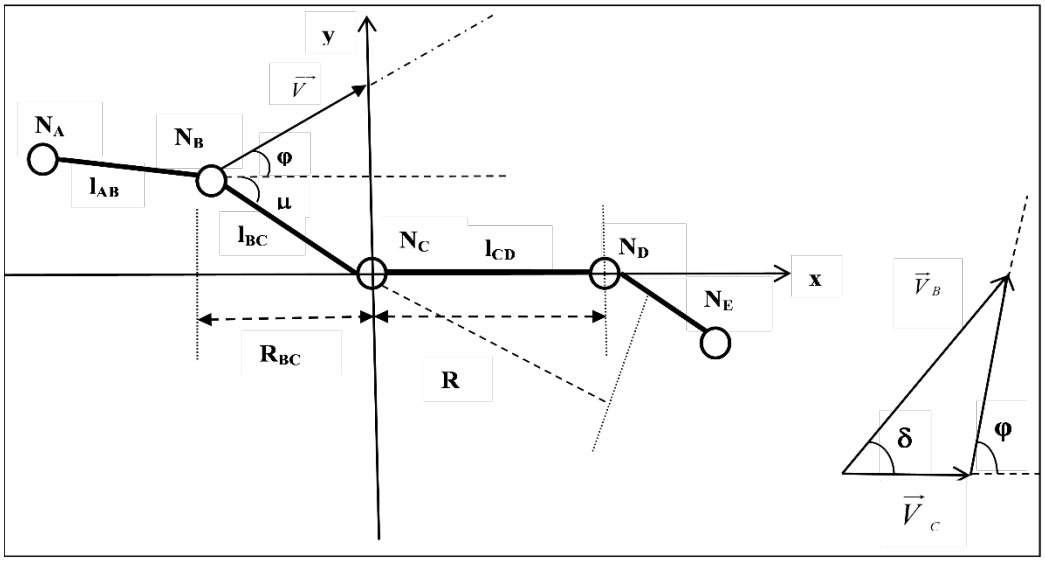

Fig. 4 *Link reliability among nodes in LSOARP*

3.2.2 Link Reliability Estimation

The link trustworthiness is computed depending on diverse mobility factors for path selection. Mobility of node at random time interval named movement interval proceeds in a steady path as well as speed depending on node movement Duration. Diverse mobility states ('N_A, N_B, N_C, N_D') are illustrated in the Figure. 4. The link trustworthiness between node 'N_B' and 'N_C' is estimated.

In Figure 4'$\overrightarrow{V_B}$' and '$\overrightarrow{V_C}$' are the speeds of nodes 'N_B', 'N_C' and '$\vec{V}$' is the qualified speed ϑ (ϑ ~U(−π, π).
μ - The angle across. '$\overrightarrow{V_B}$' and '$\overrightarrow{V_C}$'
δ - Angle among '$\vec{V}$' and '$\overrightarrow{V_C}$'
R - Node range of communication
R_{BC} - Distance between 'N_B' and 'N_C' while moving 'N_C'
L_{AB} - Link among 'N_A' and 'N_B'

Figure 4 illustrates how link reliability between nodes is calculated, taking into account factors like relative speed, direction, and distance. It also visualizes the movement patterns of multiple UAVs, providing valuable context for understanding how Residual Link Expiry (RLE) is determined.

The Residual Link Lifespan (RLE_{BC}) between 'N_B' and 'N_C' gives the logical phrase at time (T_{BC}) depending on Cumulative Distribution Function F.

$$F(RLE_{BC}(T_{BC})) = P\left[\frac{R_{BC}\cos(\delta+\mu)+\sqrt{R^2-R_{BC}^2\sin^2(\delta+\mu)}}{N_s} \leq T_{BC}\right] \quad (14)$$

If 'μ', 'R_{BC}' the original space of 'L_{BC}' is known, the arbitrariness of 'V' and 'φ' is computed using '$f_{V,\varphi}(N_{s,\varphi})$'.

$$F(RLE_{BC}(T_{BC})) = \int_{-\pi}^{\pi}\int_{w}^{V_{up}} f_v, \delta(N_s, \delta)dvd\delta \quad (15)$$

Where,

$$w = \frac{R_{BC}\cos(\delta+\mu)+\sqrt{R^2-R_{BC}^2\sin^2(\delta+\mu)}}{T_{BC}}$$

where,
V_{up} - V's upper limit of '$\overrightarrow{V_B}$' and '$\overrightarrow{V_C}$' in the specific X-axis.

$$\vec{V} = \overrightarrow{V_B} - \overrightarrow{V_C} \tag{16}$$

$$\vec{V} = V = \frac{\sqrt{Vt^2 - V_C^2 - 2V_B V_C \cos\partial}}{T_{BC}} \tag{17}$$

$$f_v, \delta(N_s, \delta) = \int \left(\frac{N_s * rV_B^m(N_{s_B}) * rV_C^n(N_{s_C})}{2\pi\sqrt{N_s^2 + N_{s_C}^2 + 2N_S.N_{S_C}.\cos\delta}} \right) dv_c \tag{18}$$

$$N_{S_B}^* = \sqrt{N_s^2 + N_{s_C}^2 + 2N_S.N_{S_C}.\cos\delta}, rV_B^m(N_{s_B}) \text{ and } rV_C^n \tag{19}$$

where,
m and n$\epsilon\{H_\varphi, I_\omega, L_\rho, P_\delta\}$.

The link trustworthiness of the former link RLE is more than the threshold 'T_{tr}'. Then Link trustworthiness of links B and C is obtained as,

$$\begin{aligned} LR_{BC} &= P(RLE_{BC} \geq T_{tr}) \\ &= 1 - F(RLE_{BC}(T_{tr})) \end{aligned} \tag{20}$$

The value of $f_v, \delta(N_s, \delta)$ is replaced in '$F(RLE_{BC}(T_{BC}))$'

Energy Efficiency

Let $P(N_0, N_K)$ be the path from the node 'N_0' to 'N_K' and it is denoted by,

$$P(N_0, N_K) = N_0, N_1, \ldots N_K \tag{21}$$

The expense of energy pathway is denoted by the '$P_{EC}(N_0, N_K)$'.

$$P_{EC}(N_0, N_K) = C(N_0, N_1) + C(N_1, N_2) + \cdots + C(N_{k-1}, N_k) \tag{22}$$

$$P_{EC}(N_0, N_K) = \sum_{i=0}^{k-1} C(N_i, N_{i-1}) \tag{23}$$

Residual Energy (RE) path $P_{RE}(N_0, N_K)$ determined while shown in the ensuing equation.

Building on that, Li et al. (2021) introduced an energy-efficient routing protocol designed to dynamically choose routes based on the battery levels of nodes and forecasts of transmission energy consumption.[20]

$$P_{RE}(N_0, N_K) = \min\left(ET(N_i) - C(N_i, N_{i-1})\right), 0 \leq i \leq K \tag{24}$$

While the source forwards the data packet to the destination, the following energy equations are considered.

$$\text{Min}\left(P_{EC}(N_0, N_k)\right) = \sum_{i=0}^{k} C(N_i, N_{i-1}) \tag{25}$$

$$\text{Max}\left(P_{RE}(N_0, N_k)\right) = P_{RE}(N_0, N_k) \tag{26}$$

The source finally selects the minimum Energy Cost (EC) path and maximum RE path. The minimum Residual Energy Path is showed below.

$$\text{Min}\left(P_{EC}(N_0, N_k)\right) = \text{Min}\left(ET - C(N_i, N_{i-1})\right) \tag{27}$$

Were,

$$ET = \frac{RE(N_i)}{Deg(N_i)} \tag{28}$$

$Deg(N_i)$ - Degree of 'N_i'
$RE(N_i)$ - Residual Energy of Ni

3.2.3 Duration of the link

To find out how long the links will be in active. we use the parameter named as Link Duration Time (Δ). Typically, two nodes have an active link if they lie within the and signals can pass through obstacles without being blocked. Without deprivation of generality, the Δ of two mobile nodes' time boundary is [tb, tb*], where 'l_{ij}' represents the node-link. Δ is given in a mathematical manner as

$$\Delta(i, j, tb) = tb^* - tb. \tag{29}$$

The mean link duration time can be measured as in (30)

$$\Delta = \frac{\sum_{t=0}^{T} \sum_{i=1}^{N} \sum_{i=i+1}^{N} \Delta(i, j, tb)}{LD} \tag{31}$$

LD is the link duration total.

3.2.4 Path Availability

The availability of a path in FANET among 2 nodes is called path availability. It refers to the amount of time a route is accessible among Node 'N_i' and 'N_j', (i,j)∈N. Due to node mobility, the process of reorganization is disrupted, thus reducing the network's performance. Path availability-dependent route selection is done to choose dependable paths. The availability of paths among pair of nodes is given as,

$$AP_c^{i,j} = \begin{cases} \frac{\sum_{t=t_{start_{i,j}}}^{T} R_{i,j}^t}{T - t_{start_{i,j}}}, \text{if } T - t_{start_{i,j}} > 0 \\ 0, \text{Otherwise} \end{cases} \tag{32}$$

were,
$R_{i,j}^t$ - It takes a value '1' if a pathway occurs from node 'N_i' to 'N_j' at time t
$t_{start_{i,j}}$ - Time of commencement of communication between 'N_i' to 'N_j'
$AP_c^{i,j}$ - Average path availability with the feasibility of communication among 'N_i' to 'N_j'.
To observe the possibility of communication in a FANET, '$AP_c^{i,j}$' averaged on node pairs is shown below.

$$AP = \sum_{i=1}^{N} \sum_{j=i+1}^{N} \frac{AP_c^{i,j}}{N_{Pair}} \tag{33}$$

Were,
N_{Pair} - Number of pairs (i,j)

3.2.5 Connectivity of Network

A metric to ensure connectivity is essential for a FANET as it determines the node's ability to maintain the link's trustworthiness level and communication. It is influenced by the node spatial distribution in 'ω'. Suppose nodes 'N_i' and 'N_j' are within similar communication limit 'r' while 2 nodes are linked depending on the following states:
Connect straight by link (l_ij), if the node distance d_ij≤r
Connect indirectly by a path (P_ij) combining a collection of links
Cooperatively connected by 'l_ij' and 'P_ij'

To observe network connectivity, let 'CY^+' and 'CY^-' refer to the connectivity and non-connectivity among node 'i' and 'j', were,

$$CY^{\pm} = \{l_{ij} \cup P_{ij}\} \tag{34}$$

$$\text{Network connectivity is shown as a random process } \{CY_t^{\pm}\}_1^j \in (1,2,..\infty,N) \tag{35}$$

The amount of the active links in '$CY_t^{\pm}$' is given by 'NL_t'.

$$NL_t = \sum_{i=1}^{N} \sum_{j=1}^{N} \frac{N_t^{ij}}{2} \tag{36}$$

were,
N_t^{ij} - Neighbor Count of node 'i' in $\{CY_t^{\pm}\}$
Network connectivity rate ($\eta(t)$) is given by,

$$\eta(t) = \frac{2NL_t}{N(N-1)} \tag{37}$$

The network develops disconnected, if $\eta(t) = 0$. Else if $\eta(t) = 1$, it means that the network is wholly connected. The ideal path calculation algorithm is described in Algorithm 2.
Figure 5 illustrates the key steps in the LSOARP decision-making process for selecting the most reliable path. It shows how the algorithm assesses neighboring nodes, updates link metrics, and refines its route choices through iterative steps.

Algorithm 2: Optimal path selection
'N_i' empty its Neighbor set NB= ϕ
For $N_j \in N[i]$
If 'N_j' provides access to node (s) in $N_2[i] \ldots N_2[I]$ - next neighbor
Eradicate 'N_j' from N[i], add 'N_j' to NB
Eliminate node(s) from $N_2[x]$ covered by 'N_j'
End if
End for
While $N_2[x]$!= ϕ
For $N_j \in N[i]$
N_i gets η_t, AP[j], TLD[j], and LR_{ij}
End for
Determine 'N_j' with max $[LR_{ij}][AP_j]\eta_t$ [TLD[j]]
If several choices exist
Determine node with max (LR_{ij}, AP_j)
Maximize 'η_t' until only one node left
If several options exist
Arbitrarily pick 'N_j' from the remaining nodes
Eliminate 'N_j' from N[i], add 'N_j' to M
End if
End if
End while

Based on the following factors such as link trustworthiness when selecting a route for data to travel from the source to the destination, factors like path availability, how long the link lasts, and how well the connection works are all considered to pick the best possible path.

J. of Soft Computing and Data Mining Vol. 6 No. 1 (2025) p. 359-377

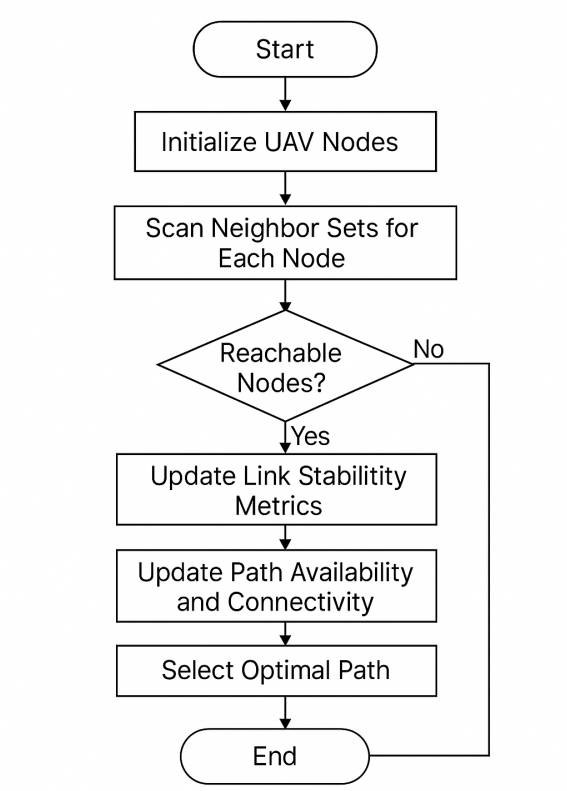

Fig. 5 *Optimal path selection*

This flowchart in Figure 5, shows how UAV networks decide the best route to take, based on what's outlined in Algorithm 2. It starts by setting up the UAV nodes and then checks each node's neighbors. If it finds reachable nodes, it updates the connection quality, the availability of paths, and how connected the network is. Using these updates, it then chooses the best route, considering factors like how reliable the links are, how long they last, energy use, and overall connectivity. If no neighbors are reachable at first, the algorithm keeps trying until new options pop up or it finds a better route. Once the best path is chosen, the process ends.

4. Results

This section dives into the performance evaluation of the proposed LSOAPR routing protocol. We simulated the protocol using the Network Simulator (NS2) and conducted a thorough analysis of its performance. Here, we detail the simulation environment, the key performance metrics used to assess LSOARP, and the results obtained from our experiment comparative study on metrics such as The analysis of control overhead, delay, energy consumption, and Packet Delivery Ratio (PDR) is performed across various source-destination pairings, velocities, node quantities, and pause durations. The efficacy of the proposed approach is evaluated against established protocols, such as the Reliable Link-Adaptive Position-Based Routing Protocol (RLPR). [21] and (AODV) [21]. Table 1 includes the parameters used in the simulation are included.

The figure number and caption should be typed below the illustration in 10pt and centered. Artwork has no text along the side of it in the main body of the text. However, if two images fit next to each other, these may be placed next to each other to save space. For example, see Fig. 1. The figures and the number should be placed in the table. Then, the table border needs to be adjusted to no border.

Table 1 *Details of the simulation*

Variable	Value
Simulant	NS-2.34
Topology area	1000 * 1000 m
Topology	Random topology
Obstacles Number	2
Nodes Number	50, 100, 150, 200 and 250
Nodes transferring speed	5- 25
Intermission duration	1, 5, 10, 20, 30 and 40
Communication range	250 m
Medium Access Control Layer	IEEE 802.11
Data Rate	2 Mbps
Transmission Model	Two Ray Ground
Physical Model	Wirelessphy
Antenna model	Omni Antenna
Traffic Type	CBR (Constant Bit Rate)
Packet Size	512 bytes
Origin-Destination pairs	5- 25
Routing Protocol	LSOARP
Preliminary Energy	100 Joules
Transfer Power	0.175 mw
Power Reception	0.175 mw
Simulation Duration	200 Sec

The parameters for our simulation, listed in Table 1, were chosen based on commonly accepted standards and benchmarks found in the literature. This helps make sure our performance evaluations are fair and that the results can be applied more broadly.

Node Counts (50–250): These numbers represent small to moderate-sized FANET environments, which are typical in real-world UAV applications like surveillance, search-and-rescue, and environmental checks. Increasing the node count gradually allows us to see how well the proposed protocol scales.

Speeds (5–25 m/s): This range reflects how fast low-altitude UAVs usually fly. It helps us test how responsive the routing protocol is under different mobility scenarios—from slow-moving surveillance to quicker patrol missions.

Pause Times (1–40 sec): These values mimic various UAV behaviors, from constant movement to frequent hovering. Analyzing how different pause durations affect link stability and path planning is important.

Communication Range (250 m): This is a typical communication distance for medium-power wireless transceivers on UAVs, providing reliable connectivity without causing too much interference or draining battery life.

Simulation Area (1000×1000 m): This area roughly matches an average urban or open-field setting where UAVs might work together.

Origin-Destination Pairs (5–25): Testing within this range allows us to see how the protocol performs under light to heavy traffic loads, especially regarding congestion, delays, and data delivery success.

We chose these parameters based on previous studies like RLPR and AODV evaluations [21][22], making it easier to compare results and demonstrate the effectiveness of our LSOARP protocol in realistic and challenging FANET situations.

Figure 6 shows how the control overhead of LSOARP compares with the RLPR and AODV protocols as the number of source-destination pairs increases. This emphasizes LSOARP's effectiveness in minimizing control messages, which is especially important in dense network environments where limited UAV resources need to be conserved and communication overhead can quickly become a bottleneck. Figure 6 varies the number of source-destination pairs and displays the control overhead. Compared to AODV and RLPR protocols, the suggested LSOARP has a control overhead that is 1.68 and 1.1 times lower, respectively.

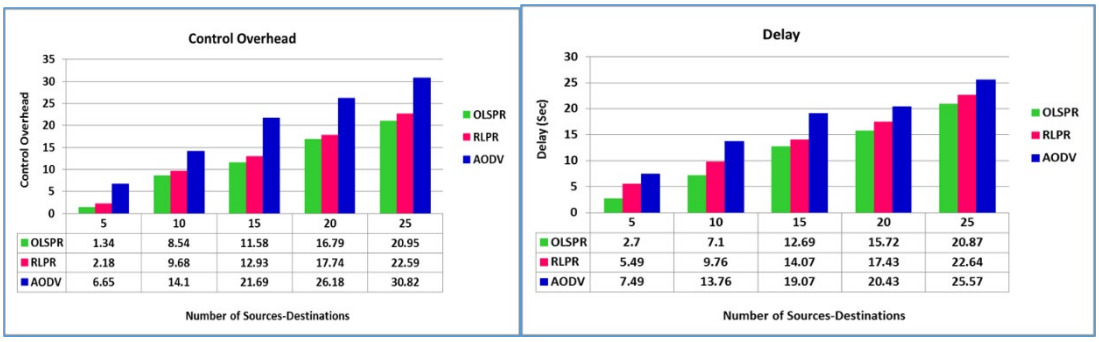

(a) **(b)**

Fig. 6 *Handling overhead for diverse quantities of sources and destinations (a);* **Fig. 7** *Latency for diverse sources and destinations (b)*

Figure 7 illustrates how the average end-to-end delay changes as the number of source-destination pairs increases. The data clearly shows that LSOARP consistently results in lower latency compared to RLPR and AODV. This advantage is primarily due to its focus on link stability and obstacle awareness, which help minimize route failures and needing retransmissions. Figure 7 Illustrates the latency for several categories of source-destination pairs. The suggested LSOARP demonstrates a delay reduction of 1.17 and 1.46 times in comparison to RLPR.

The AODV protocols are equivalent. This mostly stems from the link's dependability and the period of its usage in routing, leading to the selection of best pathways with reduced latency**.**

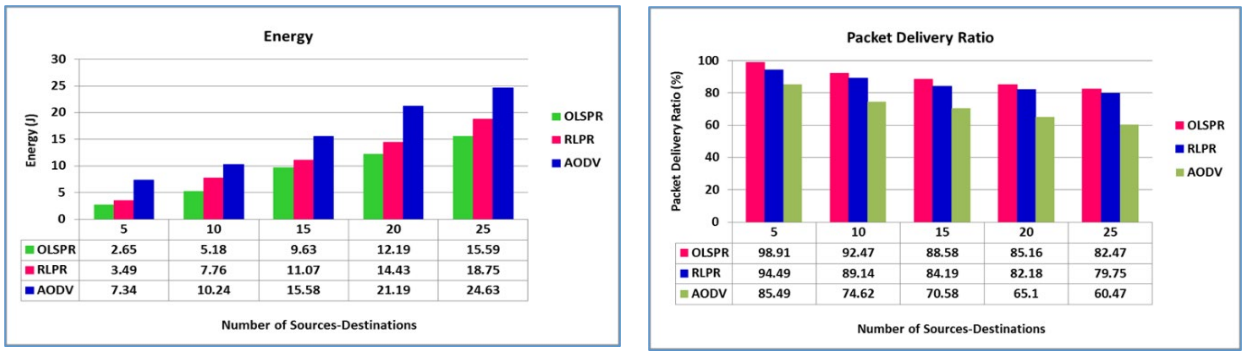

(a) **(b)**

Fig. 8 *Energy for diverse sources and destinations (a*); **Fig 9.** *Rate of packet delivery for different numbers of sources and destinations(b)*

Figure 8 illustrates the energy consumption patterns of the three routing protocols. Notably, LSOARP stands out for its ability to conserve energy by choosing efficient paths that avoid obstacles. This approach not only reduces travel time but also decreases the overall transmission effort, particularly in environments cluttered with obstacles. Figure 8 illustrates the energy consumption for different source-destination pairings. The proposed LSOARP consumes 1.23 and 1.75 times more energy than the RLPR and AODV protocols, respectively. This is attributable to our RMBC algorithm altering the trajectory from a curved path to a linear travel when no barriers impede the MN's transition from a starting position to a destination location. This decreases trip duration and consumption of energy.

Figure 9 illustrates the Packet Delivery Ratio (PDR) for different source-destination combinations. The proposed LSOARP demonstrates performance improvements of 1.04 and 1.26 times relative to the RLPR and AODV protocols, respectively. The main determinants are when choosing the best routes to avoid data loss, link stability, energy, and path availability. This enhances the proposed system's PDR, differentiating it from existing schemes.

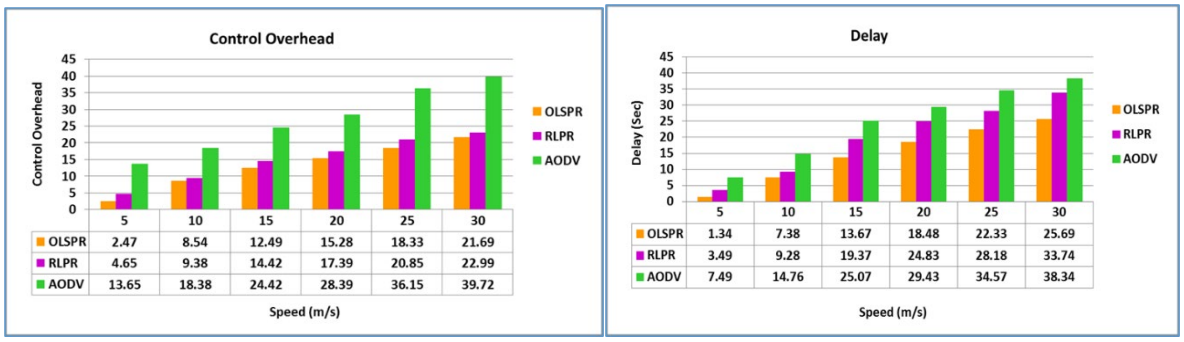

(a) **(b)**

Fig. 10 *Regulation of overhead for diverse mobility velocities (a);* **Fig 11.** *The delay for diverse mobility velocities (b)*

Figure 10 shows how the control overhead changes with different mobility speeds. the proposed LSOARP protocol reduces control overhead by about 1.14 times compared to RLPR and by 2.04 times compared to AODV. Similarly, Figure 11 shows the delay at various mobility speeds, with LSOARP providing 1.34 and 1.68 times less delay than RLPR and AODV, respectively.

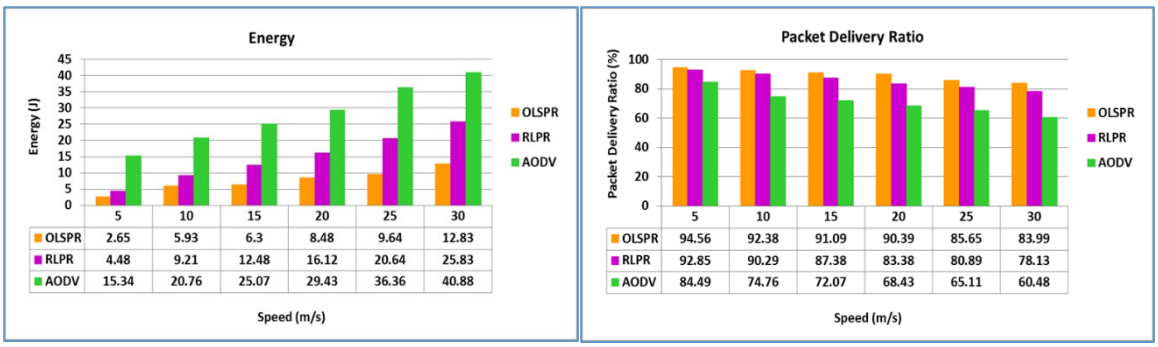

(a) **(b)**

Fig. 12 *Energy for varying mobility speeds(a);* **Fig. 13** *Packet delivery ratio for varying mobility speeds(b)*

Figure 12 represents the energy expenditure associated with different mobility velocities. The suggested LSOARP uses 1.94 to 3.66 times more energy than the RLPR and AODV protocols.
Figure 13 demonstrates the Packet Delivery Ratio (PDR) for varying mobility speeds. The proposed LSOARP offers 1.05 and 1.27 instances when contrasted to the RLPR and AODV protocols.

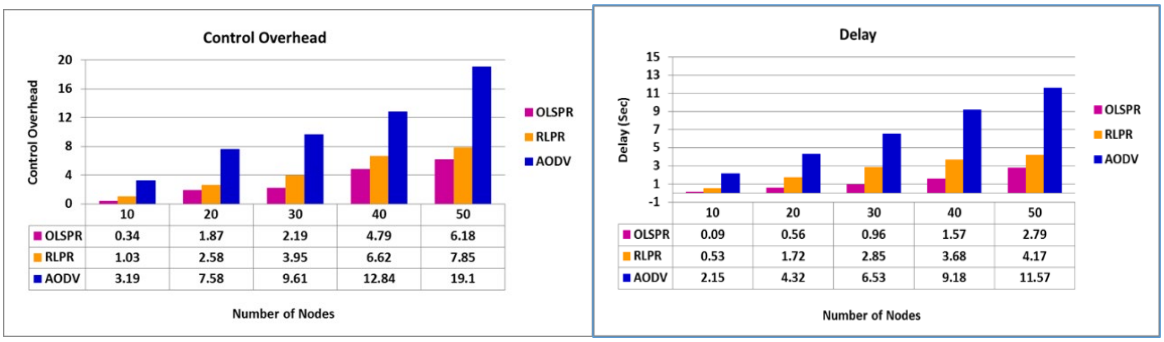

(a) **(b)**

Fig. 14 *Handling expenditure for diverse node quantities(a);* **Fig 15.** *Latency for varying number of nodes(b)*

Figure 14 demonstrates the overhead associated with many nodes. The suggested LSOARP is shown to have a control overhead that is 1.43 and 3.4 less than that of the RLPR and AODV protocols, respectively. Figure 15 Illustrates the latency for varying quantities of nodes. The suggested LSOARP demonstrates a delay reduction of 2.17 and 5.65 times compared to the RLPR and AODV protocols.

J. of Soft Computing and Data Mining Vol. 6 No. 1 (2025) p. 359-377

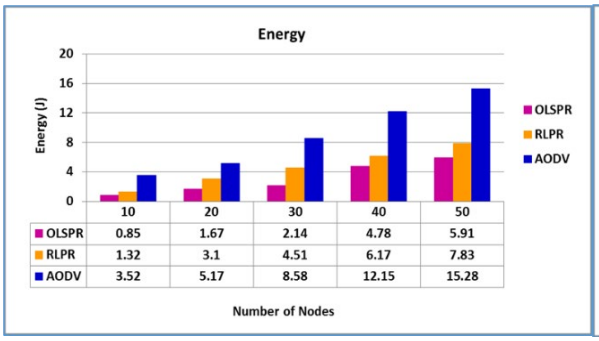

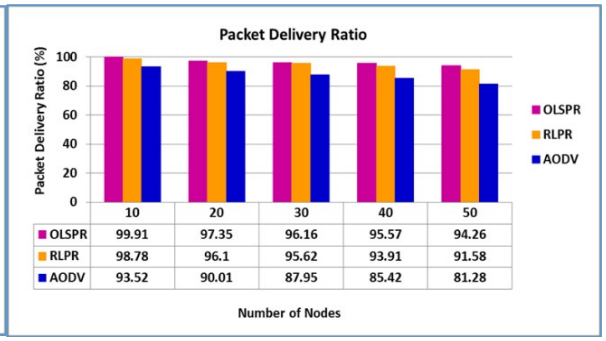

(a) **(b)**

Fig. 16 *Energy for varying number of nodes(a);* **Fig. 17** *Packet delivery ratio for varying number of nodes(b)*

Figure 16 illustrates the quantity of energy utilized for different amounts of nodes. It is observed the proposed LSOARP protocol consumes between 1.49 and 2.91 times more energy than the RLPR and AODV protocols.
Figure 17 shows the Packet Delivery Ratio (PDR) for different node ranges. Overall, LSOARP achieves slightly higher PDR, being about 1.02 to 1.10 times better compared to RLPR and AODV.

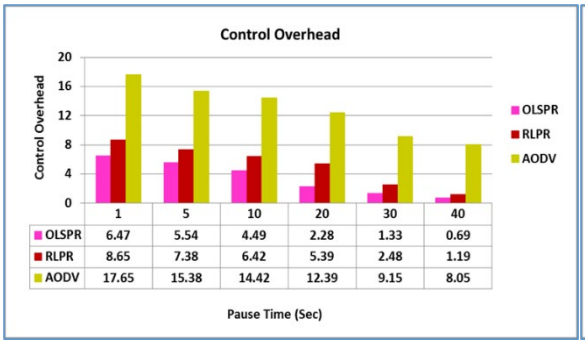

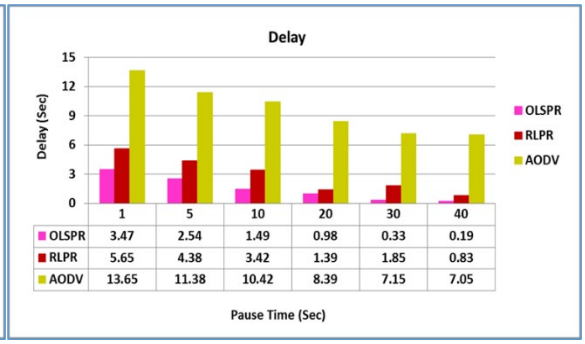

(a) **(b)**

Fig. 18 *Energy for varying number of nodes(a);* **Fig. 19** *Packet delivery ratio for varying number of nodes(b)*

Figure 18 illustrates the control overhead associated with various pause durations. The suggested LSOARP has a control overhead reduction of 1.51 and 3.7 times compared to the RLPR. and AODV protocols.
Figure 19 illustrates When looking at how long different pause times cause delays, we see that the proposed LSOARP protocol greatly reduces delay — specifically, by about 1.95 times compared to RLPR and 6.45 times compared to AODV.

Figure 20 illustrates the energy consumption corresponding to different pause durations. The projected LSOARP has been spotted use 1.27 to 2.84 times less energy than the RLPR and AODV protocols.
Figure 21 illustrates the Packet Delivery Ratio (PDR) for different pause durations. The proposed LSOARP demonstrates performance improvements of 1.03 and 1.10 times relative to the RLPR and AODV protocols, respectively. As a result of link reliability, the proposed scheme provides better PDR.

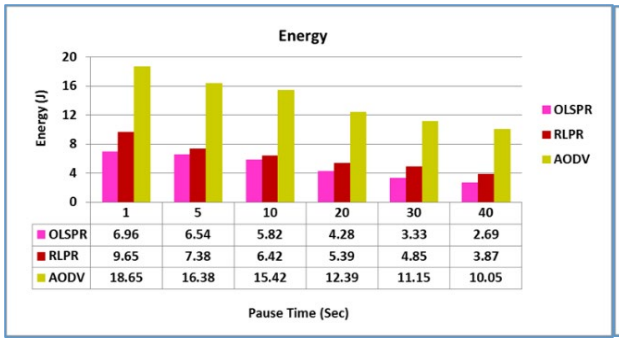

(a)

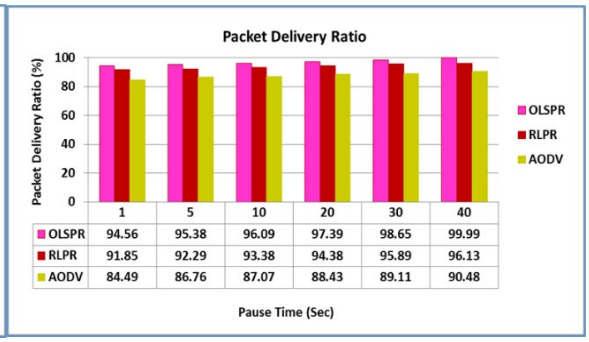

(b)

Fig. 20 *Energy for varying pause times(a);* **Fig. 21** *Packet delivery ratio for varying pause times(b)*

5. Conclusion

In this paper, we introduce LSOARP, a routing protocol designed specifically for UAV-based Flying Ad Hoc Networks (FANETs). This protocol uses Bézier curves to effectively avoid obstacles and incorporates link trust metrics—such as residual link expiry, energy levels, and connection probability—to provide reliable and efficient routing in highly energetic 3D UAV environments. We carried out extensive simulations across different scenarios, varying node speed, density, pause time, and the number of source-destination pairs. The results clearly show that LSOARP outperforms traditional protocols like RLPR and AODV, especially in terms of packet delivery ratio (PDR), energy efficiency, latency, and control overhead. These improvements mainly stem from combining obstacle avoidance with a thorough assessment of link stability, and a multi-criteria approach to path selection. That said, our study focuses on environments with static obstacles and evenly distributed node behaviours. Real-world UAV networks often face unpredictable mobility patterns, changing obstacle environments, and signal interference—factors that our current model doesn't fully cover. Besides, LSOARP doesn't yet include learning-based adaptation methods or cross-layer enhancements, which could further boost performance in complex or mission-critical scenarios. Looking ahead, we aim to develop LSOARP further by incorporating energetic obstacle modelling and reinforcement learning techniques, enabling UAVs to adapt their routing strategies based on environmental feedback. We also plan to explore integrating LSOARP with Software-Defined Networking (SDN) frameworks and 5G edge infrastructure, which could improve scalability, responsiveness, and centralized control for large-scale deployments.

Acknowledgement

The authors would like to thank the Faculty of Computer engineering Al-Farabi University Iraq, Near East University Turkey, AL-Bayan University and AL-Ain University UAE for their support.

Conflict of Interest

The authors declare that there is no conflict of interest regarding the publication of the paper.

Author Contribution

A.M, S.S: ***conceptualization, investigation, reviewing, and editing****; M.I.:* ***investigation, methodology, writing an original draft****; JO.B.:* ***research design, data analysis****; M.S, L.I.:* ***conceptualization, data curation, writing—reviewing and editing, funding acquisition, project administration****. All authors have read and agreed to the published version of the manuscript.*

References

[1] Tareque, M. H., Hossain, M. S., & Atiquzzaman, M. (2015, September). On the routing in flying ad hoc networks. In 2015 federated conference on computer science and information systems (FedCSIS) (pp. 1-9). IEEE.

[2] Khan, M. F., Yau, K. L. A., Noor, R. M., & Imran, M. A. (2019). Routing schemes in FANETs: A survey. Sensors, 20(1), 38.

[3] Lakew, D. S., Sa'ad, U., Dao, N. N., Na, W., & Cho, S. (2020). Routing in flying ad hoc networks: A comprehensive survey. IEEE Communications Surveys & Tutorials, 22(2), 1071-1120.

[4] Nadeem, A., Alghamdi, T., Yawar, A., Mehmood, A., & Siddiqui, M. S. (2018). A review and classification of flying Ad-Hoc network (FANET) routing strategies. Journal of Basic and Applied Scientific Research, 8(3), 1-8.

[5] Yang, H., & Liu, Z. (2019). An optimization routing protocol for FANETs. EURASIP Journal on Wireless Communications and Networking, 2019(1), 1-8.

[6] Chriki, A., Touati, H., Snoussi, H., & Kamoun, F. (2019). FANET: Communication, mobility models and security issues. Computer Networks, 163, 106877.

[7] Kaur, M., & Verma, S. (2020). Flying ad-hoc network (FANET): challenges and routing protocols. Journal of Computational and Theoretical Nanoscience, 17(6), 2575-2581.

[8] Hong, J., & Zhang, D. (2019). TARCS: A topology change aware-based routing protocol choosing scheme of FANETs. Electronics, 8(3), 274.

[9] Lee, S. W., Ali, S., Yousefpoor, M. S., Yousefpoor, E., Lalbakhsh, P., Javaheri, D., ... & Hosseinzadeh, M. (2021). An energy-aware and predictive fuzzy logic-based routing scheme in flying ad hoc networks (fanets). IEEE Access, 9, 129977-130005.

[10] Kumar, A., & Singh, R. (2022). Mobility and link-stability aware routing protocol for UAV ad hoc networks. *Wireless Personal Communications*, 122(3), 2147–2163. https://doi.org/10.1007/s11277-021-08926-y

[11] Oubbati, O. S., Lakas, A., Zhou, F., Güneş, M., & Yagoubi, M. B. (2017). A survey on position-based routing protocols for Flying Ad hoc Networks (FANETs). Vehicular Communications, 10, 29-56.

[12] Choi, S. C., Hussen, H. R., Park, J. H., & Kim, J. (2018, July). Geolocation-based routing protocol for flying ad hoc networks (FANETs). In 2018 Tenth international conference on ubiquitous and future networks (ICUFN) (pp. 50-52). IEEE.

[13] Zhang, Q., Feng, J., & Yang, D. (2023). Obstacle-aware position-based routing for urban UAV networks. IEEE Transactions on Vehicular Technology, 72(2), 1230–1242. https://doi.org/10.1109/TVT.2023.3241094

[14] Kumar, S., Raw, R. S., & Bansal, A. (2021). Minimize the routing overhead through 3D cone shaped location-aided routing protocol for FANETs. International Journal of Information Technology, 13(1), 89-95.

[15] Gankhuyag, G., Shrestha, A. P., & Yoo, S. J. (2017). Robust and reliable predictive routing strategy for flying ad-hoc networks. IEEE Access, 5, 643-654

[16] Kim, G. H., Mahmud, I., & Cho, Y. Z. (2017, December). Self-recovery scheme using neighbor information for multi-drone ad hoc networks. In 2017 23rd Asia-Pacific Conference on Communications (APCC) (pp. 1-5). IEEE.

[17] Sorbelli, F. B., Corò, F., Das, S. K., Palazzetti, L., & Pinotti, C. M. (2022). Drone-based optimal and heuristic orienteering algorithms towards bug detection in orchards. In 18th Int. Conf. on Distr. Computing in Sensor Systems (DCOSS)(submitted). IEEE

[18] Páleš, Dušan & Rédl, Jozef. (2015). BEZIER CURVE AND ITS APPLICATION. Mathematics in Education, Research and Applications. 01. 49-55.10.15414/meraa.2015.01.02.49-55

[19] Raj, V., & Gupta, S. (2021). Real-time obstacle-aware path planning for UAVs using terrain mapping and sensor-based prediction. Journal of Intelligent & Robotic Systems, 103(4), 65–78. https://doi.org/10.1007/s10846-021-01385-2

[20] Li, Y., Wang, H., & Zhao, L. (2021). An energy-efficient routing strategy for UAV ad hoc networks. *Ad Hoc Networks*, 123, 102607. https://doi.org/10.1016/j.adhoc.2021.102607

[21] Usman, Qamar & Chughtai, Omer & Qadri, Nadia & Kaleem, Zeeshan & Khaliq, Kishwer & Nguyen, Long. (2021). A Reliable Link-Adaptive Position-Based Routing Protocol for Flying ad hoc Network. Mobile Networks and Applications. 26. 10.1007/s11036-021-01758-w.

[22] van Glabbeek, R., Höfner, P., Portmann, M. et al. Modelling and verifying the AODV routing protocol. Distrib. Comput. 29, 279–315(2016). https://doi.org/10.1007/s00446-015-0262-7